WILEY-VCH

The Biomolecular Corona in 2D and Reverse: Patterning Metal–Phenolic Networks on Proteins, Lipids, Nucleic Acids, Polysaccharides, and Fingerprints

*Gyeongwon Yun[+], Joseph J. Richardson[+], Marco Capelli, Yingjie Hu, Quinn A. Besford, Alessia C. G. Weiss, Hojae Lee, Insung S. Choi, Brant C. Gibson, Philipp Reineck, and Frank Caruso**

Dr G. Yun, Dr. J. J. Richardson, Y. Hu, Dr. Q. A. Besford, Dr. A. C. G. Weiss, Prof. F. Caruso
ARC Centre of Excellence in Convergent Bio-Nano Science and Technology, and the Department of Chemical Engineering, The University of Melbourne, Parkville, Victoria 3010, Australia

M. Capelli, Prof. B. C. Gibson, Prof. P. Reineck
ARC Centre of Excellence for Nanoscale BioPhotonics and School of Science, RMIT University, Melbourne, Victoria 3001, Australia

H. Lee, Prof. I. S. Choi
Center for Cell-Encapsulation Research, Department of Chemistry, KAIST, Daejeon 34141, Republic of Korea

Keywords: metal–organics, sensing, forensics, thin films, protein corona

The adsorption of biomolecules onto nanomaterials can alter the performance of the nanomaterials in vitro and in vivo. Recent studies primarily focus on the protein "corona", formed upon adsorption of proteins onto nanoparticles in biological fluids, which can change the biological fate of the nanoparticles. Conversely, interactions between nanomaterials and other classes of biomolecules namely lipids, nucleic acids, and polysaccharides have received far less attention despite their important roles in biology. A possible reason for this is the challenge associated with investigating biomolecule interactions with nanomaterials using current technologies. Herein, a protocol is developed for studying bio–nano interactions by depositing four classes of biomolecules (proteins, lipids, nucleic acids, and polysaccharides) and complex biological media (blood) onto planar substrates, followed by exposure to metal–phenolic network (MPN) complexes. The MPNs preferentially interact with the biomolecule over the inorganic substrate (glass), highlighting that patterned biomolecules can be used to engineer patterned MPNs. Subsequent formation of silver nanoparticles on the MPN films maintains the patterns and endows the films with unique reflectance and fluorescence properties, enabling visualization of latent fingerprints (i.e., invisible residual biomolecule patterns). This study demonstrates the potential complexity of the biomolecule corona as all classes of biomolecules can adsorb onto MPN-based nanomaterials.

1. Introduction

Understanding the interactions between nanosized materials and organisms is driving developments in applications, such as targeted drug delivery, and mitigation of the environmental impact of nanomaterials.[1-3] Biomolecules are known to adsorb onto nanomaterials and thereby alter the physicochemical properties and biological fate of the nanomaterials. However, the biomolecule corona field has almost exclusively focused on the protein corona formed around nanoparticles entering biological media (e.g., serum, blood).[4] For example, albumin, the most

abundant protein in blood, with a concentration of ~40 g L^{-1} (~600 μM), adsorbs in high quantities on most materials entering the bloodstream.[5] In contrast, fewer studies have investigated how the other three major classes of biomolecules namely lipids,[6-9] nucleic acids, and polysaccharides[10-12] interact with nanomaterials in the context of the biomolecule corona though these biomolecules are regularly adsorbed onto nanoparticles.[13] Many gel and mass spectrometry techniques have been optimized to accurately quantify the size and amino acid composition of proteins.[14] However, the other three classes of biomolecules are more difficult to study and quantify accurately, as there are only 20 amino acids with distinct molecular compositions, whereas other types of biomolecules have a much wider range of chemical compositions, molecular weights, and branching structures.[14] Although less abundant, these other three classes of biomolecules control many processes at the femto–nanomolar range,[15] suggesting that these could play an equally important role in governing bio–nano interactions and therapeutic outcomes. Moreover, the concentration and composition of these three classes of biomolecules vary widely in media at any given time. For example, meals can drastically alter both the polysaccharide and lipid content in blood,[16] whereas tumor cells often release trace amounts of nucleic acids into the bloodstream during growth and metastasis.[17, 18] A further issue limiting the comprehensive understanding of the biomolecule corona are the challenges associated with studying biomolecule adsorption on particulate nanomaterials due to the complexities of handling, separating, and purifying nanoparticles.[19] Alternatively, macroscopic substrates are in many cases more amenable to study bio–nano interactions.

Metal–phenolic networks (MPNs) are an emerging class of universally adherent organic–inorganic hybrid nanomaterials composed of phenolic ligands chelated with metal ions.[19, 20] Phenolic molecules can interact with nearly any material owing to their dendritic composition of multiple

catechol/galloyl groups capable of interacting with surfaces through electrostatic interactions, hydrogen bonding, hydrophobic interactions, and π–π stacking. Phenolic molecules have been used historically to precipitate proteins in the winemaking process[21] and tan leather in the tanning industry.[22] However, their interactions with other biomolecules are less explored. Similarly, the specific interaction of MPNs with different biomolecules has not been investigated though MPNs show promise in diverse fields, including drug delivery, bioimaging, and cytoprotection.[23, 24] Herein, we demonstrate that tannic acid (TA)/iron (Fe^{III}) MPNs can interact with all four major classes of biomolecules (proteins, lipids, nucleic acids, and polysaccharides). Instead of studying the adsorption of these biomolecules onto MPN-coated nanoparticles, a "reverse" approach was adopted, wherein the biomolecules of interest were deposited onto planar supports and the preferential growth of MPNs on the biomolecule patterns (**Figure 1**) was studied. An MPN growth time of approximately 24 h was necessary for direct visualization of the biomolecule patterns by eye. However, by reducing silver nanoparticles (AgNPs) onto the MPNs in situ, similar to our previous reports on AgNP synthesis on MPNs,[25] patterns were visualized after an MPN growth time of only 1 h owing to enhanced reflectance and fluorescence properties owing to the AgNPs in the films. The preferential growth of the MPNs on the biomolecules over the planar substrate also allowed for the visualization of natural biomolecule patterns, including clean fingerprints invisible to the naked eye (latent and uncharged) or fingerprints deposited after gently rubbing the face (charged) with resolution down to single sweat pores (the gold standard for forensic profiling).[26] First-person action cameras[27] were used to document the experimental protocol to facilitate replication and build on this work. The present work highlights that all four classes of biomolecules can interact with MPNs and is anticipated to underpin and initiate studies on the more complete

biomolecule corona for nanomaterials, rather than the corona of a single class of biomolecules using the reverse corona.

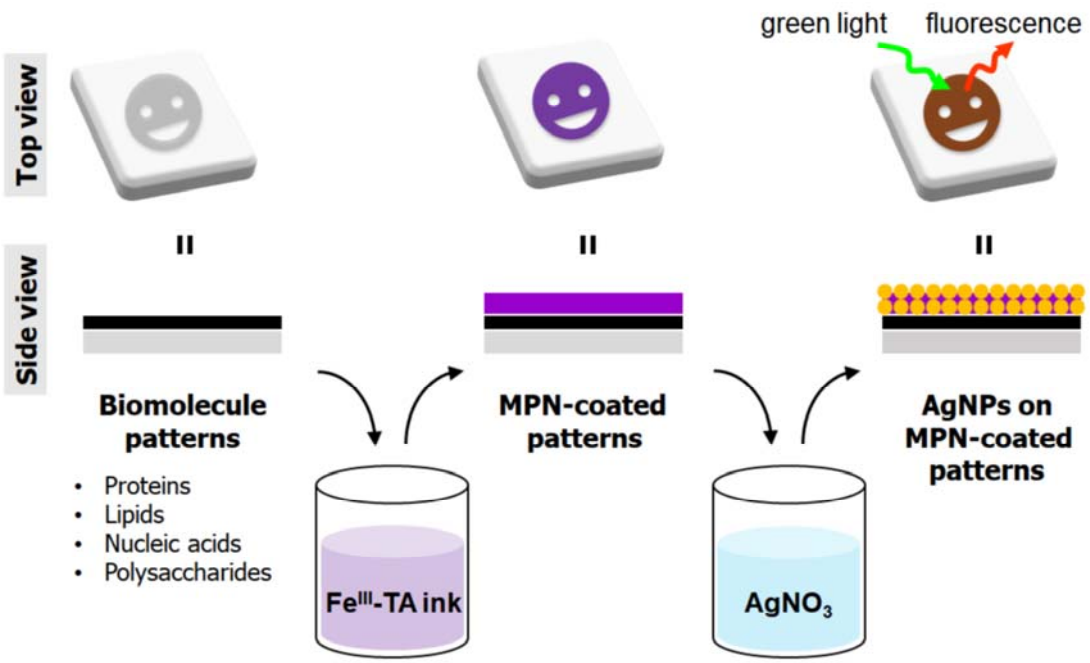

Figure 1. Schematic illustration showing the preferential deposition of MPNs on biomolecule patterns (over the substrate) and subsequent AgNP formation for enhanced visualization of the biomolecule pattern using fluorescence.

2. Results and Discussion

2.1. MPN Growth on Biomolecule Patterns

We first investigated whether MPNs could preferentially deposit on the substrate or the following four major classes of biomolecules: proteins, lipids, nucleic acids, and polysaccharides. The biomolecule-patterned planar glass substrates were prepared by dip-pen lithography with either protein (bovine serum albumin, BSA), lipids (1,2-dimyristoyl-*sn*-glycero-3-phosphocholine and 1,2-dipalmitoyl-*sn*-glycero-3-phosphocholine), nucleic acid (ssDNA (40mer)), or polysaccharide (dextran) solutions, all at ~10 mg mL^{-1}. The biomolecule patterns were invisible to the naked eye

after evaporation of the solvents (chloroform for the lipids, and water for BSA, DNA, and dextran) under ambient conditions (**Figure 2**a–d). MPN films were prepared using our recently published protocol,[25] which leads to controlled, time-dependent film growth of thickness of ~10–5000 nm. Briefly, a concentrated aqueous solution of TA (40 mg mL^{-1}) was mixed with an equal volume of aqueous $FeCl_3$ solution (10 mg mL^{-1}) and used as is (see **Movie S1**, Supporting Information). Notably, the biomolecule patterns were visible after immersion for 24 h in the MPN solution, as seen by eye (Figure 2e–h, see **Movie S2**, Supporting Information) and as indicated by the characteristic ligand-to-metal charge transfer (LMCT) band in the UV–visible (UV–vis) absorption spectrum (**Figure 3**o). The appearance of the patterns indicated that the growth rate of the MPN film on the biomolecule pattern was faster than on the bare substrate. This result highlights that though ubiquitously adherent films can grow on all substrates,[28] their growth rate can be modulated by biomolecule patterns. Interestingly, the MPN patterns were visible for lipids that are solid at room temperature (left side of Figure 2f), but not easily visible for lipids that are liquid at room temperature (right side of Figure 2f). Although the MPNs grew on all of the biomolecules, the relative growth followed the trend of solid lipids > proteins > polysaccharides > DNA > liquid lipids, based on the specific biomolecules of each class tested herein. Interestingly, the detection threshold varied for two common proteins, namely BSA and hemoglobin, with detection limits of 0.015 mg mL^{-1} and 0.00015 mg mL^{-1}, respectively (**Figure S5**). These results not only demonstrate that MPNs can be macroscopically patterned using biomolecules, but also demonstrate that the MPNs have different sensitivities depending on both the biomolecule class and the specific biomolecule. This has implications for biomedical applications of MPNs, such as biomolecule detection, where specific biomolecules could potentially be isolated from blood with MPNs.

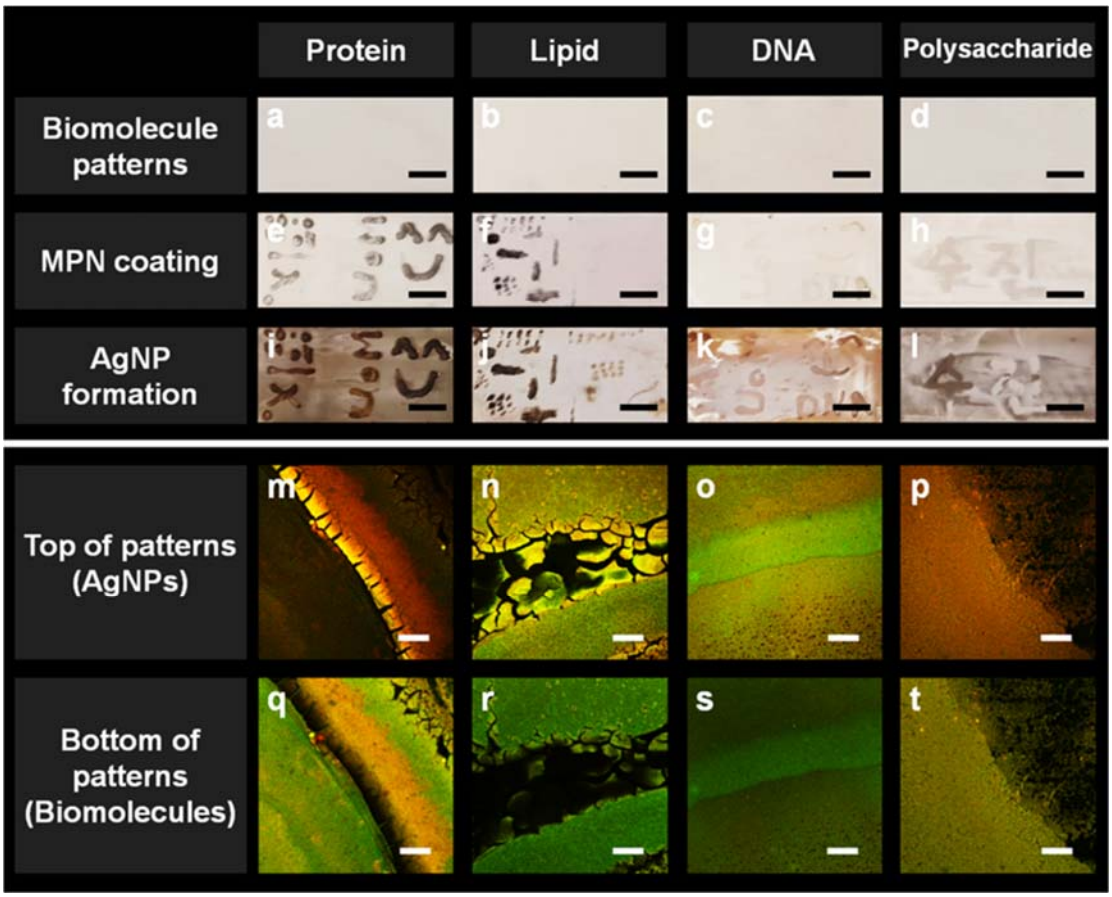

Figure 2. (a–l) Digital photographs and (m–t) confocal fluorescence images of biomolecule patterns, MPN-coated biomolecule patterns, and AgNP-coated MPN patterns. (a–d) Biomolecule patterns on glass. (e–h) MPN films on the biomolecule patterns after immersion of the patterns in MPN solution for 24 h. (i–l) AgNPs decorated on the MPN patterns after immersion of the MPN-coated biomolecule patterns in $AgNO_3$ solution for 24 h. (m–t) Fluorescence images of top (m–p) and bottom (q–t) of the AgNP-coated MPN patterns, where the biomolecules exhibit green fluorescence due to labeling with fluorophores that are excited by a blue laser (i.e., 488 dyes) and the AgNPs show red fluorescence. Scale bars are (a–l) 1 cm and (m–t) 100 μm.

2.2. MPN Growth on Fingerprints

Fingerprints are unique natural micro/macropatterns composed of a variety of biomolecules depending on the genetics and environment of the bearer.[29] We therefore explored whether MPNs could be selectively grown on fingerprint patterns. We deposited charged and uncharged fingerprints from different donors on a variety of substrates (glass, metal, plastic, and paper). The latent uncharged fingerprints became partially visible after 6 h of MPN growth and were fully visible at 24 h (**Figure S1**). The MPN growth process was independent of a specific ratio of biomolecules as it occurred on different prints from different donors (**Figure S2**) and was partially independent of the substrate type as fingerprints were developed on a variety of materials depending on whether the fingerprints were charged. Namely, latent fingerprints were visualized on glass, and charged fingerprints were also visualized on paper, plastic, and metal (**Figure S3**). Furthermore, fingerprint patterns were detected by using other MPN assembly methods. For example, charged fingerprints on a glass substrate developed by stamping the substrate on MPN films formed at the air–water interface (**Figure S4**).[30] However, careful observation under differential interference contrast (DIC) microscopy revealed relatively low-fidelity replication of the micro-patterns of the fingerprints (i.e., sweat pores and eyes) (**Figure 3**). Thus, methods were investigated to enhance the visualization of the patterns.

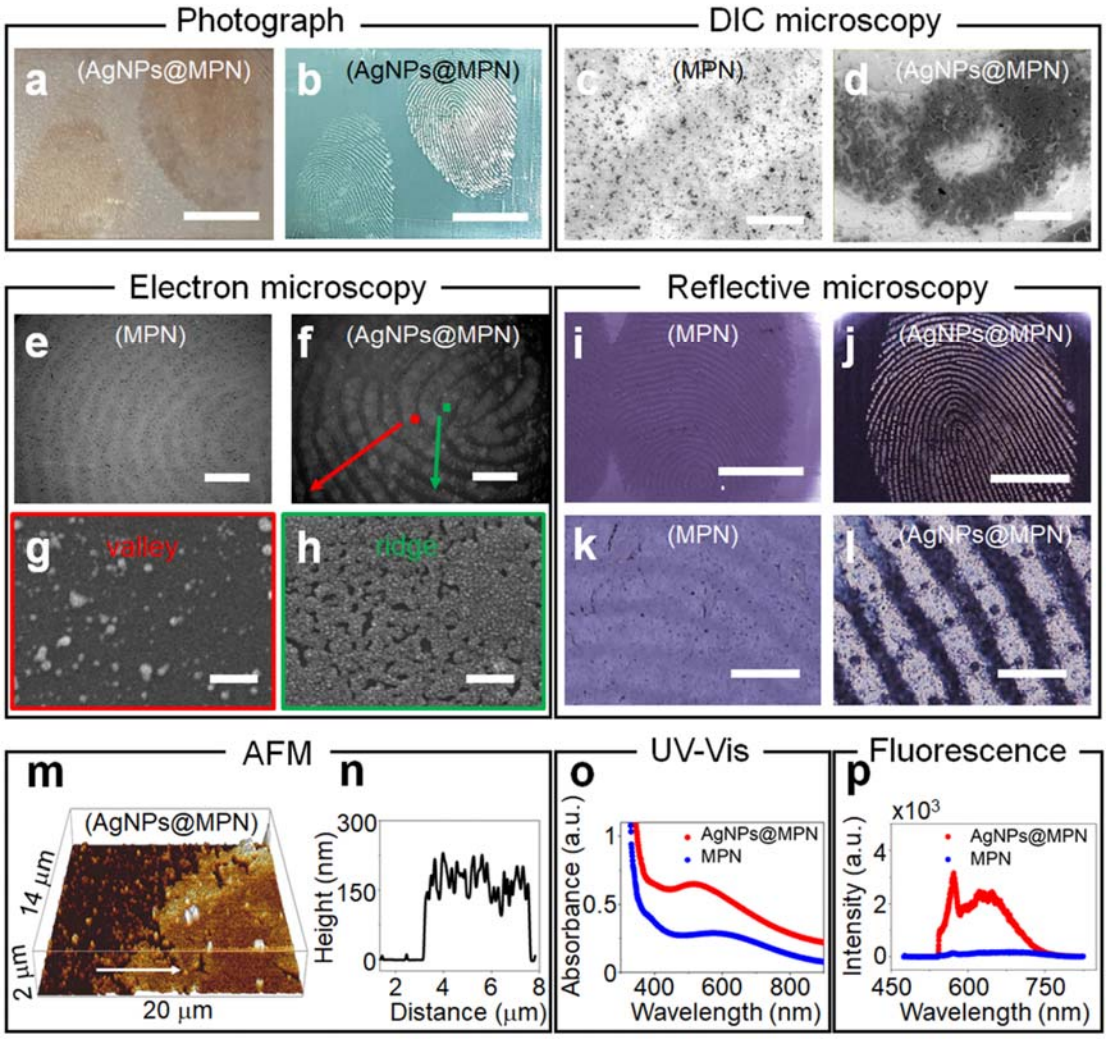

Figure 3. Characterization of fingerprint patterns (c,e,i,k,n,o) after MPN deposition and subsequent AgNP formation (a,b,d,f,g,h,j,l,m,n,o,p), highlighting that natural biomolecule patterns (i.e., fingerprints) can be visualized after nanofilm growth imaged with a variety of experimental techniques, including (a,b) digital photography with a cell phone (without (a) and with (b) a flash), (c,d) DIC microscopy, (e–h) scanning electron microscopy (SEM), (i–l) reflectance microscopy, and (m, n) atomic force microscopy (AFM). (o) UV–Vis absorption spectra and (p) fluorescence emission spectra (excitation wavelength = 525 nm) of the films before and after AgNP formation

on MPN-coated fingerprints. Scale bars are (a,b) 1 cm, (c,d) 200 μm, (e,f) 1 mm, (g,h) 1 μm, (i,j) 0.5 cm, and (k,l) 400 μm.

2.3. AgNP Formation on Patterned MPNs for Enhanced Visualization

The natural ability of TA to reduce metal ions into metal NPs is retained when TA is incorporated into MPNs,[25] thereby offering a potential means to increase the visibility of the patterned MPNs. First, we investigated the formation of AgNPs on the MPN-coated biomolecule patterns by immersing the MPN-coated biomolecule patterns in $AgNO_3$ solution for 24 h. A noticeable blue shift in the absorption band of the patterns was observed by UV–vis spectroscopic analysis, suggesting in situ formation of AgNPs (Figure 3o,p). Moreover, the purple color of the MPN pattern became brownish after AgNP growth, making the patterns easier to visualize by eye (Figure 2i–l). Interestingly, the previously invisible liquid MPN-coated lipid pattern became visible after AgNP formation (right side of Figure 2j). In addition, visualization of the MPN-developed latent fingerprint patterns was enhanced through AgNP formation (Figure 3a and b, and Figure S1 and S2, see **Movie S3** and **S4**, Supporting Information). Inspired by the visualization of previously invisible patterns (lipids that are liquid at room temperature), we investigated whether AgNPs could be formed on the MPN-coated latent fingerprints that were invisible to the naked eye (i.e., films grown for less than 6 h). As observed from Figure S1, not only did the MPN fingerprints become visible after only 1 h of MPN growth (immersion in $AgNO_3$ for 24 h, Figure S1), but also only 1 h of AgNP formation was necessary for visualization (MPN growth for 24 h, **Figure S6**). In addition, the detection limit improved by an order of magnitude for BSA from 0.015 mg mL^{-1} to 0.0015 mg mL^{-1}, again highlighting that invisible patterns after MPN coating become visible after AgNP formation (Figure S5). Moreover, the fingerprints could easily be "lifted" from the substrates using tape (**Figure S7**). Scanning electron microscopy revealed selective growth of the AgNPs (average

size of ~60 nm as imaged by SEM and AFM (Figure 3h, m), and confirmed by small-angle X-ray scattering, **Figure S8**) on the fingerprint ridge, with minimal formation on the fingerprint valley (Figure 3e–h). AFM measurements confirmed this selective growth, showing that the final height of the MPN-coated fingerprint was ~150–250 nm after MPN growth for 24 h and AgNP formation after 24 h (Figure 3m). Importantly, the AgNP formation was unique to the MPN-coated biomolecule patterns, as biomolecule patterns alone, or coated with polymerized TA or TA monolayers did not yield any visible patterns after silver treatment (**Figure S9**). These results demonstrate that MPNs not only are useful for biomolecule patterning, but also could potentially be used as an invisible TA-ink detector.

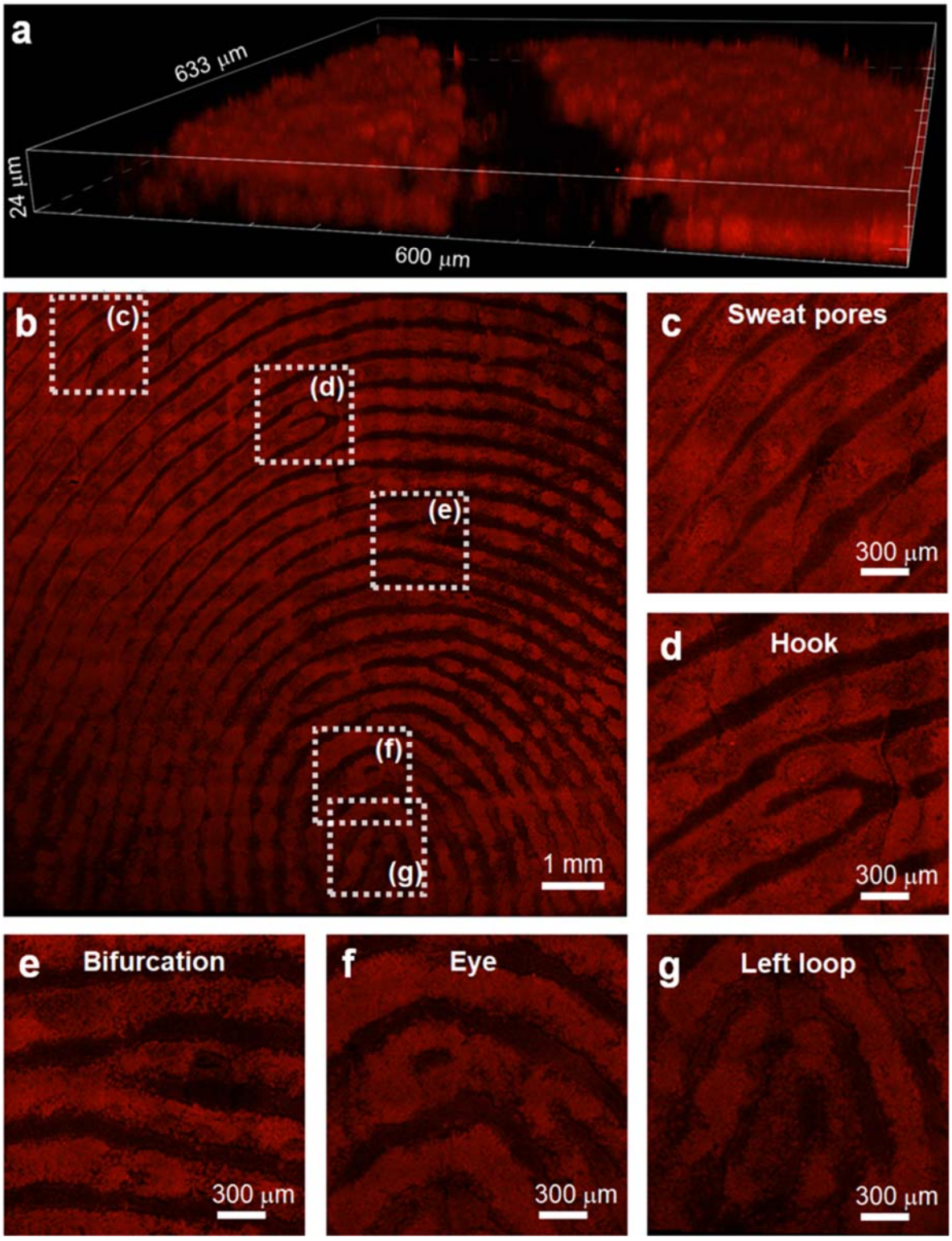
a
633 μm
24 μm
600 μm
b
(c)
(d)
(e)
(f)
(g)
1 mm
c
Sweat pores
300 μm
d
Hook
300 μm
e
Bifurcation
300 μm
f
Eye
300 μm
g
Left loop
300 μm

Figure 4. Confocal fluorescence images of AgNPs on an MPN-coated latent fingerprint on glass excited with a 561 nm laser with data collected in the range of ~570–800 nm. (a) 3D composite of confocal slices, (b) overview of the pattern at a single focal plane, and (c–g) second-level details (d,e,g) and third-level details (c,f) of the fingerprint with the technical forensic feature names in each box.

Finally, the AgNP-patterned films were more thoroughly investigated on the microscopic level—the finest details of the latent fingerprints were easily visualized under a light microscope equipped with a 20× objective. The high scattering of the AgNPs allowed for the use of reflectance imaging (Figure 3b) and reflectance microscopy (Figure 3j and l, and Figure S3), highlighting the ease of high-fidelity visualization. Moreover, the presence of sub-100 nm NPs (Figure S8) and the UV–vis peak at ~530 nm (Figure 3o) prompted additional investigation on the fluorescence properties of the AgNPs grown on the MPN patterns.[31] A sharp emission peak was seen at 572 nm together with a broad band in the range of 550–800 nm (excitation wavelength = 525 nm) (Figure 3p).[32] The peak at 572 nm (1552 cm^{-1}) is a Raman feature of the phenolic molecules.[33, 34] However, the presence of AgNPs enhanced the Raman signal[34] by more than an order of magnitude when compared with the signal obtained for the MPN-coated fingerprints without the AgNPs (**Figure S10**). The total emission signal allowed for high-resolution fluorescence imaging using confocal fluorescence microscopy equipped with a 561 nm excitation laser, with emission in the red–far-red region (**Figure 4**).[31] Both reflectance microscopy and fluorescence microscopy facilitated the observation of forensic-specific fingerprint pattern features with second and third-level details including sweat pores, bifurcation, eye, hook, and loop (Figure 3j and 3l, and 4b–g).[35] Moreover, this fluorescence allowed for visualization of the location of the AgNPs@MPN in relation to the biomolecule patterns, demonstrating that for the protein and polysaccharide patterns, the

AgNPs@MPNs were spatially on top of the biomolecules, whereas for the lipid and DNA patterns they were interpenetrated throughout the uppermost strata of the biomolecule pattern (Figure 2m–t). This suggests that the diverse interactions between the biomolecules and MPN precursors, such as chelation of Fe^{3+} with the backbone of DNA and the hydrophobic interactions between lipids and TA, can dictate how and where the MPNs will form on the biomolecule patterns. Overall, the growth of AgNPs on the MPN patterns provides a platform for multimodal imaging with high spatial resolution, relevant for forensics and potentially relevant for biomedicine.

2.4. MPN Growth on Patterns of Complex Biological Fluids

As a final proof of concept, complex biological media relevant for both the biomedical and forensic fields was used for patterning. Fingerprints prepared from human blood were deposited on different substrates (paper, cloth, glass, metal, and plastic) and either immediately immersed in MPN precursor solution or left to dry before MPN growth. Owing to the abundance of biomolecules and cells in blood and the presence of iron the MPNs initially grew too rapidly and uncontrolled on the blood prints. Thus, the concentration was halved (17×10^{-3} M iron(III) chloride hexahydrate and 12×10^{-3} M TA) to improve the sensitivity. Still, the MPNs rapidly deposited on the prints (within 5 s), where longer incubation periods (10 s) resulted in more MPN growth for wet prints (**Figures S11** and **S12**). However, lower concentrations (8.5×10^{-3} M iron(III) chloride hexahydrate and 6×10^{-3} M TA) did not allow for the rapid development of the prints (Figure S12). The prints could also be visualized after drying on both plastic and metal (**Figures S13** and **S14**), highlighting the versatility of this approach for growing MPNs on patterns of complex biological fluids.

3. Conclusion

In conclusion, we demonstrated that MPNs preferentially grow on proteins, lipids, nucleic acids, or polysaccharides over the glass substrate, which allows for the macroscopic and microscopic

patterning of MPNs. Natural biomolecule patterns, e.g., fingerprints, were replicated down to the sweat pore level (on the order of ~100 μm) upon MPN coating and subsequent AgNP formation on the patterned MPNs for enhanced visualization using reflectance microscopy and fluorescence microscopy. As MPNs are typically below a few micrometers in thickness,[25, 30, 36, 37] the present high-fidelity resolution of replication suggests that a similar approach could potentially be used for sub-micrometer patterns. Still, some limitations could exist for reverse corona experiments, as the biomolecules are first adsorbed onto a substrate and therefore substrate-effects and reconfiguration are possible. Ideally, the corona would be as straightforward to study as the reverse corona for non-protein biomolecules; however, the reverse corona is currently the most feasible general screening method and should be applicable to various nanoparticles and nanomaterials other than MPNs. Finally, it should be noted that the future of the biomolecule corona will likely evolve past the four major classes of biomolecules studied herein to eventually contain complex bio entities such as extracellular vesicles, exosomes, viruses, and cellular debris. Moreover, the true corona present in vivo could potentially also contain environmental contaminants, such as small molecules, minerals, and heavy metals, which will further complicate our understanding of the formation of the corona around nanomaterials but will be crucial for bolstering the predictive qualities of ex vivo tests.

4. Experimental Section

Formation of Biomolecule Patterns: Biomolecule solutions (10 mg mL^{-1}, lipid in chloroform, and BSA, DNA, or dextran in water) were prepared. A clean and dry micropipette tip was soaked in the biomolecule solution and subsequently used as a pen to sketch the patterns on glass. The biomolecule patterns were then left to dry under ambient conditions. No washing was performed.

Formation of Fingerprints: Fingerprints were either deposited after hand washing and drying (latent and uncharged) or after gently rubbing the face (charged). All fingerprints were deposited by healthy adult subjects.

MPN Growth: For the formation of MPN films, aqueous solutions of iron(III) chloride hexahydrate (37×10^{-3} M, 10 mL) and TA (24×10^{-3} M, 10 mL) were separately prepared in deionized water. These two solutions were then combined and mixed by a vortex mixer for 10 s. The biomolecule patterns were then immersed in the mixed solution for 1 min–24 h. The MPN-coated biomolecule patterns were washed with deionized water to remove excess tannic acid/iron and dried under a stream of dry air.

AgNP Formation on the MPN Patterns: According to our previous report,[25] the MPN-coated biomolecule patterns were immersed in silver nitrate solution (37×10^{-3} M, 20 mL) for 1 min–24 h. The AgNP-coated MPN patterns were washed with deionized water to remove the excess silver nitrate and dried under a stream of dry air. Finally, the samples were kept in the dark prior to analysis.

Fingerprint Patterning with Biological Fluids and Subsequent MPN Formation: Prints with blood were gently deposited on a wide variety of substrates including paper, cloth, metal, glass, and plastic and either processed while wet or after drying. MPNs were grown on the prints at different concentrations with a fixed Fe^{3+}-to-TA ratio (namely ~3:2, with ideal concentrations of 17×10^{-3} M for iron(III) chloride hexahydrate and 12×10^{-3} M for TA) and for different time points (5 or 10 s). After MPN growth, the prints were washed gently with deionized water and dried with a stream of air. Human Research and Ethics Committee approval (1750753.1) was obtained for all studies of human samples, and informed signed consent was obtained from the subjects.

Supporting Information

Supporting Information is available from the Wiley Online Library or from the author.

Acknowledgements

[+]G.Y. and [+]J.J.R. contributed equally to this work. This research was conducted and funded by the Australian Research Council (ARC) Centre of Excellence in Convergent Bio-Nano Science and Technology (project number CE140100036), the ARC Centre of Excellence for Nanoscale BioPhotonics (project number CE140100003), and an ARC Discovery Project (DP170103331). This work was partly conducted on the SAXS beamline of the Australian Synchrotron, part of ANSTO. This work was performed in part at the Materials Characterization and Fabrication Platform (MCFP) at The University of Melbourne and the Victorian Node of the Australian National Fabrication Facility (ANFF). F.C. acknowledges the award of a National Health and Medical Research Council Senior Principal Research Fellowship (GNT1135806). P.R. acknowledges funding through the RMIT Vice Chancellor's Research Fellowship. M.C. acknowledges the support of a PhD scholarship from the ARC Centre of Excellence for Nanoscale BioPhotonics and RMIT University. I.S.C. acknowledges the support of the Basic Science Research Program through the National Research Foundation of Korea (NRF) funded by the Ministry of Science, ICT & Future Planning (MSIP2012R1A3A2026403).

References

[1] M. P. Monopoli, C. Åberg, A. Salvati, K. A. Dawson, *Nat. Nanotechnol.* **2012**, *7*, 779.

[2] D. Docter, D. Westmeier, M. Markiewicz, S. Stolte, S. Knauer, R. Stauber, *Chem. Soc. Rev.* **2015**, *44*, 6094.

[3] M. Markiewicz, J. Kumirska, I. Lynch, M. Matzke, J. Köser, S. Bemowsky, D. Docter, R. Stauber, D. Westmeier, S. Stolte, *Green Chem.* **2018**, *20*, 4133.

[4] P. C. Ke, S. Lin, W. J. Parak, T. P. Davis, F. Caruso, *ACS Nano* **2017**, *11*, 11773.

[5] M. Hadjidemetriou, Z. Al-Ahmady, M. Mazza, R. F. Collins, K. Dawson, K. Kostarelos, *ACS Nano* **2015**, *9*, 8142.

[6] A. A. Kapralov, W. H. Feng, A. A. Amoscato, N. Yanamala, K. Balasubramanian, D. E. Winnica, E. R. Kisin, G. P. Kotchey, P. Gou, L. J. Sparvero, *ACS nano* **2012**, *6*, 4147.

[7] G. Hu, B. Jiao, X. Shi, R. P. Valle, Q. Fan, Y. Y. Zuo, *ACS Nano* **2013**, *7*, 10525.

[8] S. S. Raesch, S. Tenzer, W. Storck, A. Rurainski, D. Selzer, C. A. Ruge, J. Perez-Gil, U. F. Schaefer, C.-M. Lehr, *ACS Nano* **2015**, *9*, 11872.

[9] E. Hellstrand, I. Lynch, A. Andersson, T. Drakenberg, B. Dahlbäck, K. A. Dawson, S. Linse, T. Cedervall, *FEBS J.* **2009**, *276*, 3372.

[10] Z. Zeng, J. Patel, S.-H. Lee, M. McCallum, A. Tyagi, M. Yan, K. J. Shea, *J. Am. Chem. Sci.* **2012**, *134*, 2681.

[11] S. Zhang, Y. Moustafa, Q. Huo, *ACS Appl. Mater. Interfaces* **2014**, *6*, 21184.

[12] S. Wan, P. M. Kelly, E. Mahon, H. Stöckmann, P. M. Rudd, F. Caruso, K. A. Dawson, Y. Yan, M. P. Monopoli, *ACS Nano* **2015**, *9*, 2157.

[13] J. J. Richardson, J. W. Maina, H. Ejima, M. Hu, J. Guo, M. Y. Choy, S. T. Gunawan, L. Lybaert, C. E. Hagemeyer, B. G. De Geest, *Adv. Sci.* **2015**, *2*, 1400007.

[14] K. Cai, A. Z. Wang, L. Yin, J. Cheng, *J. Controlled Release* **2017**, *263*, 211.

[15] A. K. Vaishnaw, J. Gollob, C. Gamba-Vitalo, R. Hutabarat, D. Sah, R. Meyers, T. de Fougerolles, J. Maraganore, *Silence* **2010**, *1*, 14.

[16] G. Schaafsma, W. Meuling, W. Van Dokkum, C. Bouley, *Eur. J. Clin. Nutr.* **1998**, *52*, 436.

[17] H. Schwarzenbach, D. S. Hoon, K. Pantel, *Nat. Rev. Cancer* **2011**, *11*, 426.

[18] P. S. Mitchell, R. K. Parkin, E. M. Kroh, B. R. Fritz, S. K. Wyman, E. L. Pogosova-Agadjanyan, A. Peterson, J. Noteboom, K. C. O'Briant, A. Allen, *Proc. Natl. Acad. Sci. USA* **2008**, *105*, 10513.

[19] M. A. Rahim, S. L. Kristufek, S. Pan, J. J. Richardson, F. Caruso, *Angew. Chem.* **2019**, *131*, 1920; M. A. Rahim, S. L. Kristufek, S. Pan, J. J. Richardson, F. Caruso, *Angew. Chem. Int. Ed. Engl.* **2019**, *58*, 1904.

[20] H. Ejima, J. J. Richardson, F. Caruso, *Nano Today* **2017**, *12*, 136.

[21] B. Sun, I. Spranger, F. Roque-do-Vale, C. Leandro, P. Belchior, *J. Agr. Food Chem.* **2001**, *49*, 5809.

[22] A. D. Covington, *Chem. Soc. Rev.* **1997**, *26*, 111.

[23] J. Guo, Y. Ping, H. Ejima, K. Alt, M. Meissner, J. J. Richardson, Y. Yan, K. Peter, D. von Elverfeldt, C. E. Hagemeyer, *Angew. Chem.* **2014**, *126*, 5652; J. Guo, Y. Ping, H. Ejima, K. Alt, M. Meissner, J. J. Richardson, Y. Yan, K. Peter, D. von Elverfeldt, C. E. Hagemeyer, *Angew. Chem. Int. Ed. Engl.* **2014**, *53*, 5546.

[24] J. H. Park, K. Kim, J. Lee, J. Y. Choi, D. Hong, S. H. Yang, F. Caruso, Y. Lee, I. S. Choi, *Angew. Chem.* **2014**, *126*, 12628; J. H. Park, K. Kim, J. Lee, J. Y. Choi, D. Hong, S. H. Yang, F. Caruso, Y. Lee, I. S. Choi, *Angew. Chem. Int. Ed. Engl.* **2014**, *53*, 12420.

[25] G. Yun, Q. A. Besford, S. T. Johnston, J. J. Richardson, S. Pan, M. Biviano, F. Caruso, *Chem. Mater.* **2018**, 30, 5750.

[26] A. K. Jain, Y. Chen, M. Demirkus, *IEEE Trans. Pattern Anal. Mach. Intell.* **2007**, *29*, 15.

[27] M. Björnmalm, M. Faria, F. Caruso, *Chem. Mater.* **2016**, *28*, 8441.

[28] H. Lee, S. M. Dellatore, W. M. Miller, P. B. Messersmith, *Science* **2007**, *318*, 426.

[29] Z. Zhou, R. N. Zare, *Anal. Chem.* **2017**, *89*, 1369.

[30] H. Lee, W. I. Kim, W. Youn, T. Park, S. Lee, T. S. Kim, J. F. Mano, I. S. Choi, *Adv. Mater.* **2018**, *30*, 1805091.

[31] Y. Ishida, R. Nakabayashi, R. D. Corpuz, T. Yonezawa, *Colloids Surf., A* **2017**, *518*, 25.

[32] A. S. Lee, P. J. Mahon, D. C. Creagh, *Vib. Spectrosc.* **2006**, *41*, 170.

[33] J. Spanget-Larsen, M. Gil, A. Gorski, D. M. Blake, J. Waluk, J. G. Radziszewski, *J. Am. Chem. Sci.* **2001**, *123*, 11253.

[34] Z. Jurasekova, A. Torreggiani, M. Tamba, S. Sanchez-Cortes, J. Garcia-Ramos, *J. Mol. Struct.* **2009**, *918*, 129.

[35] E. Tabassi, P. Grother, in *Encyclopedia of Biometrics* (Eds S. Z. Li, A. K. Jain), Springer, New York, **2009**, p. 482.

[36] M. A. Rahim, M. Björnmalm, N. Bertleff-Zieschang, Q. Besford, S. Mettu, T. Suma, M. Faria, F. Caruso, *Adv. Mater.* **2017**, *29*, 1606717.

[37] C. Maerten, L. Lopez, P. Lupattelli, G. Rydzek, S. Pronkin, P. Schaaf, L. Jierry, F. Boulmedais, *Chem. Mater.* **2017**, *29*, 9668.

The interaction of specific biomolecules with nanomaterials is important for various applications but can be challenging to study. Metal–phenolic networks can be selectively grown on four major classes of biomolecules, where subsequent growth of silver nanoparticles allows for enhanced detection and visualization. Using this technique, biomolecule patterns, including latent and blood-based fingerprints, can be visualized in detail.

Biomolecule detection

G. Yun[+], J. J. Richardson[+], M. Capelli, Y. Hu, Q. A. Besford, A. C. G. Weiss, H. Lee, I. S. Choi, B. C. Gibson, P. Reineck, and F. Caruso*

The Biomolecular Corona in 2D and Reverse: Patterning Metal–Phenolic Networks on Proteins, Lipids, Nucleic Acids, Polysaccharides, and Fingerprints